JACS
JOURNAL OF THE AMERICAN CHEMICAL SOCIETY
pubs.acs.org/JACS
Article

Desuccinylation-Triggered Peptide Self-Assembly: Live Cell Imaging of SIRT5 Activity and Mitochondrial Activity Modulation

Liu Yang,◇ Raoul Peltier,◇ Manman Zhang,◇ Dan Song, Hui Huang, Ganchao Chen, Ying Chen, Fanghang Zhou, Quan Hao, Liming Bian, Ming-liang He,* Zuankai Wang,* Yi Hu,* and Hongyan Sun*

Cite This: J. Am. Chem. Soc. 2020, 142, 18150−18159

ABSTRACT: Mimicking nature's ability to orchestrate molecular self-assembly in living cells is important yet challenging. Molecular self-assembly has found wide applications in cellular activity control, drug delivery, biomarker imaging, etc. Nonetheless, examples of suborganelle-confined supramolecular self-assembly are quite rare and research in this area remains challenging. Herein, we have presented a new strategy to program supramolecular self-assembly specifically in mitochondria by leveraging on a unique enzyme SIRT5. SIRT5 is a mitochondria-localized enzyme belonging to a family of NAD$^+$-dependent histone deacetylases. Accumulating studies suggest that SIRT5 is involved in regulating diverse biological processes, such as reactive oxygen defense, fatty acid metabolism, and apoptosis. In this study, we designed a novel class of succinylated peptide precursors that can be transformed into self-assembling building blocks through SIRT5 catalysis, leading to the formation of supramolecular nanofibers in vitro and in living cells. The increased hydrophobicity arising from self-assembly remarkably enhanced the fluorescence of nitrobenzoxadiazole (NBD) in the nanofibers. With this approach, we have enabled activity-based imaging of SIRT5 in living cells for the first time. Moreover, SIRT5-mediated peptide self-assembly was found to depolarize mitochondria membrane potential and promote ROS formation. Coincubation of the peptide with three different chemotherapeutic agents significantly boosted the anticancer activities of these drugs. Our work has thus illustrated a new way of mitochondria-confined peptide self-assembly for SIRT5 imaging and potential anticancer treatment.

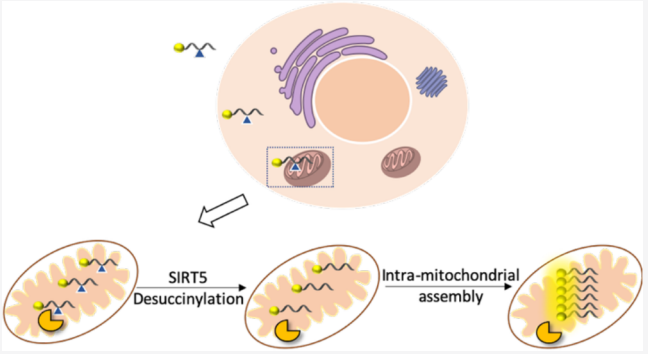

INTRODUCTION

Molecular self-assembly is a critical event occurring in many biological processes, such as intracellular transport, cell motion, and muscle contraction. Mimicking nature's innate ability opens a new route to create and engineer various synthetic molecules that can self-assemble to form functional materials in living organisms.[1,2] Such molecular self-assembly approach can be used for a wide range of biological applications, including cellular activity control, drug delivery, biosensing, tissue engineering, antimicrobial material design, and others.[3−7] Extensive efforts have been spent in manipulating self-assembly in nonliving systems. Nevertheless stimuli-responsive and spatiotemporally controlled self-assembly in living systems remains challenging. It demands precise engineering and rigorous control over the involved intermolecular forces, which are often combinations of hydrophobic interactions, electrostatic interactions and hydrogen bonding, in complex cellular environment.[8]

A conventional approach to controlling supramolecular events uses short peptides that are designed to self-assemble in response to chemical or physical triggers, such as pH, enzymes or redox reactions.[9−11] By designing appropriate peptide precursors, small-scale chemical reactions occurring in cells can be amplified via the stimuli-triggered self-assembly process to create supramolecular nanostructures. Among the different triggering methods, Xu's group pioneer the field of enzymatic-instructed self-assembly (EISA). Their approaches are particularly successful at promoting intracellular nanofiber formation under enzymatic catalysis.[12] By selecting enzymes (e.g., alkaline phosphatase) that are overexpressed in cancer cells, the methods can be used to kill cancer cells with good selectivity.[13,14]

Despite these tremendous developments, achieving spatiotemporally controlled self-assembly to target specific suborganelles is still challenging. One of the popular approaches relies on using targeting groups, such as nuclear localization sequence (NLS) or cholesterol moiety.[15] For instance, Xu et

Received: August 6, 2020
Published: September 29, 2020

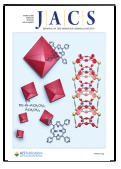

https://dx.doi.org/10.1021/jacs.0c08463
J. Am. Chem. Soc. 2020, 142, 18150−18159

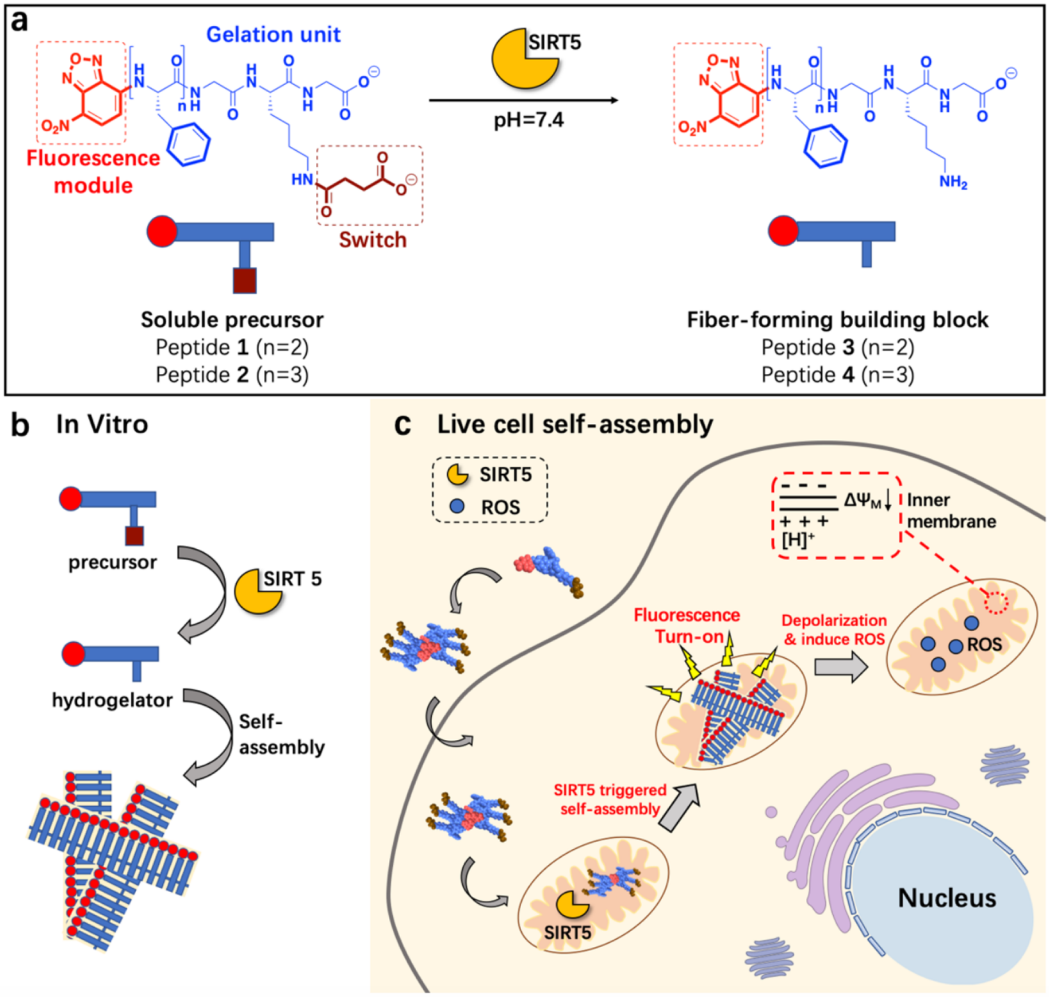

Figure 1. Mitochondria-restricted self-assembly of peptide nanofibers catalyzed by SIRT5. (a) Molecular structures of precursors and fiber-forming building blocks. Peptide precursors **1** and **2** can be desuccinylated by SIRT5 to produce fiber-forming building blocks **3** and **4**, respectively. (b) Schematic representation of the self-assembly process triggered by SIRT5 in vitro. (c) Schematic representation of intracellular fiber formation in mitochondria via specific interaction of internalized peptide precursors with SIRT5 enzyme.

al. and Ryu et al. have independently employed a triphenyl phosponium (TPP) moiety as the mitochondria-targeting group to form nanofibers specifically in the mitochondria of cells. The strategy induced mitochondria dysfunction and killed cancer cells selectively.[16,17] In another approach, Xu et al. have designed an elegant method to form nanofibers selectively in mitochondria through the combined use of a protease (enterokinase) and a branched peptide. The branched peptide was able to target mitochondria. Therefore, this strategy has enabled delivery of anticancer drugs and even proteins into mitochondria.[18,19] Yang et al. have designed a coassembly of peptide-drug amphiphile and cisplatin.[20] Due to the positively charged cisplatin, the complex formed was able to target nucleus and exhibited enhanced cytotoxicity to cancer cells and improved antitumor efficiency. Other notable examples include using L-homoarginine and cholesterol to target endoplasmic reticulum (ER) and lipid rafts of membrane, respectively.[21,22] These researches have tremendously inspired the development of innovative strategies for self-assembly that targets suborganelles. Nevertheless, self-assembling approaches utilizing enzymes with specific localization to achieve subcellular targeting remain much less explored. In light of the exquisite substrate specificity and specific localization of certain enzymes, we envision that such a strategy may greatly enhance the specificity of self-assembly targeting suborganelles.

Sirtuin proteins belong to a family of class III NAD^+-dependent histone deacetylase enzymes, which have emerged as attractive therapeutic targets. They are involved in regulating a wide range of biological processes such as aging, gene transcription, inflammation and apoptosis.[23] Sirtuin family consists of seven isoforms (SIRT1-SIRT7). Among them, SIRT5 is a mitochondrial enzyme and displays efficient protein lysine desuccinylase, demalonylase and deglutarylase activities.[24−26] Biological studies have shown that SIRT5 is involved in regulating diverse biological processes including tricarboxylic acid cycle, reactive oxygen defense, fatty acid metabolism and apoptosis.[27] A recent study has shown that SIRT5 might contribute to colorectal carcinogenesis.[28] These studies highlight the roles of SIRT5 as a promising anticancer drug target. As a mitochondrial enzyme,[29] SIRT5 can be a potential candidate to control desuccinylation and subsequent self-assembly of the proteins/peptides in mitochondria. SIRT5-mediated self-assembly of fluorescent peptide precursors can be used for imaging cellular SIRT5 in an activity-based fashion. To the best of our knowledge, designing chemical probes for

https://dx.doi.org/10.1021/jacs.0c08463
J. Am. Chem. Soc. 2020, 142, 18150−18159

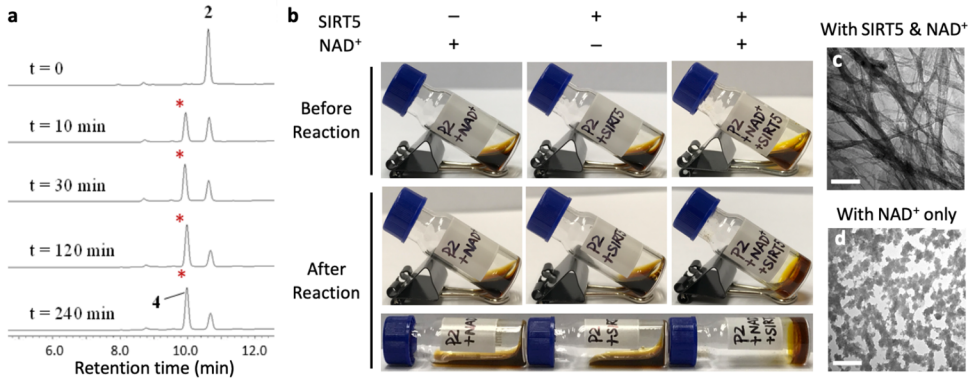

Figure 2. Nanofibers and hydrogel formation induced by SIRT5-catalyzed enzymatic desuccinylation process. (a) HPLC monitoring of the desuccinylation reactions of peptide **2** (1 mM) in the presence of 0.005 equiv SIRT5 and 2 equiv NAD^+ in TRIS buffer (pH = 7.4). *denotes the newly formed product; (b) Hydrogelation behavior of peptide **2** with NAD^+, SIRT5, and SIRT5 and NAD^+ respectively. The peptide was incubated under different conditions for 16 h and hydrogel formation was observed. (c) TEM image of peptide **2** incubated with SIRT5 and NAD^+ overnight. (d) TEM image of peptide **2** incubated overnight with NAD^+ only. The scale bar of TEM imaging is 200 nm. These results unambiguously proved that SIRT5 is capable of desuccinylating peptide **2** and triggering the nanofiber formation of peptide **2** under aqueous condition.

tracking SIRT5 activity in mammalian cells is challenging and such probes are still lacking.

In this study, we hypothesize that SIRT5 could act as a unique biological trigger and induce mitochondria-confined supramolecular self-assembly. Through rational design, we successfully synthesized peptide precursors that can selectively respond to SIRT5 and self-assemble to form nanofibers. The peptide precursors mainly consist of three parts (Figure 1a): an environment-sensitive fluorophore NBD for imaging, a phenylalanine-rich peptide fragment, and a Ksucc (succinylated lysine) switch module. Previous study has shown that fluorophore NBD can produce bright fluorescence when it is in a hydrophobic nanofiber environment.[30,31] The phenylalanine-rich peptide fragment is incorporated because aromatic interaction is favored to form self-assembling nanofibers. The Ksucc switch is designed to have multiple functions by delicately controlling the surface charge and the hydrophobicity of the peptide precursors: 1. The carboxylic acid group of Ksucc increases the solubility of the precursors in aqueous environment. 2. The negative charge of Ksucc decreases self-assembly due to electrostatic repulsion. 3. The hydrophobicity and the charge of Ksucc can be selectively modulated by SIRT5 enzyme.

We hypothesize that the amphipathic peptide precursors with low molecular weight will allow efficient internalization and diffusion within cells.[32,33] On the other hand, the amphipathic peptide precursors could aggregate themselves in cellular environment to facilitate cell entry (Figure 1c). Upon reaching the mitochondrial region of the cells, the negatively charged Ksucc in the peptide will be hydrolyzed and transformed into the positively charged lysine residue by SIRT5 enzyme, leading to the formation of desuccinylated peptide with zero charge. This unique zwitterionic nature of individual peptide building blocks promotes electrostatic interactions between each other, thereby facilitating the collective self-assembly process. The self-assembly process is further strengthened by the enhanced hydrophobicity as a result of the cleavage of the hydrophilic group during the hydrolysis process. Moreover, the NBD in the as-formed nanofibers will produce strong fluorescence due to the hydrophobic environment, allowing fluorescent detection or imaging of cellular SIRT5 activity. Importantly, the intracellular self-assembly occurred in mitochondria might serve as a useful tool for modulating mitochondrial activity, providing a useful approach for mitochondria-targeted cancer therapy.

RESULTS

Design and Synthesis of Peptide Precursors. We started by designing a total of four peptides containing either two (1) or three (2) phenylalanine residues (Figure 1a) with and without succinylation. The peptide sequences are NBD-FFGKsuccG (**1**), NBD-FFFGKsuccG (**2**), NBD-FFGKG (**3**), and NBD-FFFGKG (**4**), respectively. Succ denotes succinylation modification. Peptides **3** and **4** were first synthesized using standard Fmoc strategy. After obtaining peptide **3** and **4**, the two peptides were reacted with excess succinic anhydride in solution to produce peptide **1** and **2**, respectively (Scheme S1). The crude peptides were then purified via high-performance liquid chromatography (HPLC). The targeted peptides with the desired succinylation sites were successfully obtained. The peptides were of high purity, as evidenced by HPLC and mass spectrometry measurements (Figure S1).

SIRT5-Triggered Self-Assembly of Peptide Precursors in Vitro. After successfully synthesizing the peptides, we first examined whether they were enzymatically responsive to SIRT5. Peptides **1** and **2** showed comparable conversion in the presence of 0.005 equiv SIRT5 and 2 equiv NAD^+ (Figures 2a and S2). More than half of peptide **1** was desuccinylated after 10 min at pH 7.4 (Figure 2a). By contrast, both peptides remained unchanged without the addition of enzyme, suggesting that the desuccinylation depends on the biocatalysis of SIRT5 (Figures S2 and S3a). The selectivity of the enzymatic reaction was further assessed by incubating peptide **2** with different enzymes, including both SIRT1, an enzyme from the sirtuin family but with distinctive substrate preference, and esterase, a destructive enzyme with hydrolase activity. Results showed that peptide **2** was stable in the presence of these two enzymes (Figures S3b,c). Taken together, these results proved that the peptide precursor designed can be desuccinylated by SIRT5 and show high specificity toward SIRT5.

Subsequently, we performed the gelation experiment to examine whether the peptides could form supramolecular

https://dx.doi.org/10.1021/jacs.0c08463
J. Am. Chem. Soc. 2020, 142, 18150−18159

nanostructures under the catalysis of SIRT5. After incubating a concentrated solution of peptide **2** (1 wt %, 12 mM) with 0.005 equiv SIRT5 and 2 equiv NAD^+, the initial pure liquid solution was transformed into a solid-like gel of yellow color (Figure 2b). The formation of gel is a typical signature for the generation of nanoscale fiber networks. It should be noted that the formation of hydrogel demands a critical gelation concentration (1 wt %, Figure S4), above which the entanglement of nanofibers as well as the entrapping of a large number of water molecules can result in highly hydrated material, i.e. hydrogel.[34,35] To confirm the formation of nanofibers, we further carried out transmission electron microscopy (TEM) measurement. The TEM images clearly revealed a network of entangled fibers with diameters ranging from approximately 10 to 50 nm (Figure 2c). In the control experiments conducted under similar conditions but without using SIRT5 enzyme or NAD^+, no hydrogel was formed (Figure 2b). Moreover, TEM showed an amorphous structure (Figure 2d and S5). These results strongly proved that the formation of nanofiber is attributed to the selective interaction between SIRT5 and the peptide.

Further gelation experiment was carried out with peptide **1**. Surprisingly, no gel was formed after peptide **1** was incubated with enzyme and cofactor (Figure S6), which was further confirmed by TEM microscopy (Figure S7). This result could be ascribed to the decreased supramolecular interactions (e.g., hydrogen bonding and aromatic−aromatic stacking) resulting from the loss of one phenylalanine residue in its precursor. Taken together, these results proved our design and revealed the delicate balance in hydrophobicity required to induce SIRT5-triggered gel formation. In addition, a peptide (NBD-FGGGKG) with the same length as peptide **4** but different sequence failed to form hydrogel under the same conditions (Figure S8), further proving that peptide sequence is important for hydrogelator design.[36,37]

We next performed the imaging study of NBD-containing peptide in the gel using confocal fluorescence microscopy. Figure S9a shows the fluorescence image of peptide **2** incubated with SIRT5 and NAD^+ overnight. Bright fluorescent spots with micrometer sizes could be clearly observed and distinguished from the background. The fluorescent signal was ascribed to the strong emission of NBD dyes, which were densely localized in the hydrophobic environment of the nanofibers.[30,31] In contrast, no noticeable fluorescence was observed in the control sample without SIRT5 (Figure S9b), suggesting the validity of using NBD dye to detect the formation of nanofibers. Moreover, distinct from gelation and TEM visualization, the fluorescence measurement provides an alternative tool for real time imaging of supramolecular nanostructures.

SIRT5-Triggered Self-Assembly of Peptide Precursors in Living Cells. Encouraged by these results, we next examined the feasibility of self-assembly of supramolecular nanostructures in living cells. HeLa cells expressing SIRT5 enzyme were chosen in our study. Briefly, peptide **2** at concentrations of 50 μM and 500 μM were respectively incubated with HeLa cells. The fluorescence intensity of the cells was monitored using confocal fluorescence microscopy (Figures 3 and S10). Figure 3 shows the representative microscopy images of peptide **2** at different concentrations. Cells incubated with 50 μM peptide **2** for 6 h showed weak intracellular fluorescence (Figure 3b), whereas cells incubated with 500 μM peptide **2** displayed significant intracellular

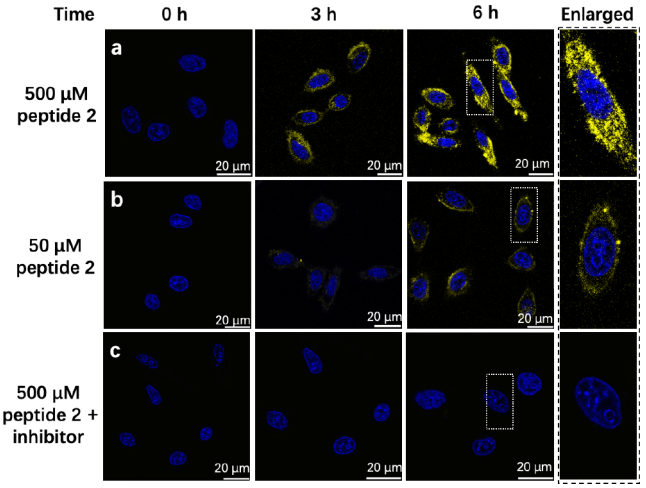

Figure 3. SIRT5-triggered self-assembly in HeLa cells. Fluorescence confocal microscopy images of HeLa cells at various time points after incubation with (a) 500 μM peptide **2**, (b) 50 μM peptide **2**, and (c) 500 μM peptide **2** + 300 μM SIRT5 inhibitor. Hoechst 33342 (20 μg/mL) was used for nucleus staining. Scale bar = 20 μm. Experiments showed that cells treated with high concentration of peptide **2** displayed bright fluorescence, signifying that supramolecular structures were formed in living cells. Cells treated with SIRT5 inhibitor did not show fluorescence, indicating that SIRT5 is the key player responsible for nanofiber formation.

fluorescence (Figure 3a). The manifestation of strong fluorescence inside the cell incubated with high concentration of peptide **2** signified the occurrence of nanosized fibers (Figure 3a).[30,31] For the cells incubated with low concentrations of peptide **2**, the production of self-assembling building block was not sufficient to form nanofibers. Consequently, no significant fluorescence was observed.

Peptide **1** was tested as a negative control that reacts with SIRT5 but does not form nanofibers. As expected, HeLa cells incubated with 500 μM peptide **1** did not show any fluorescence after 6 h of incubation (Figure S11, top image). Surprisingly, direct incubation of HeLa cells with peptide **4** did not produce intracellular fluorescence (Figure S11, bottom image). Instead, small aggregates could be observed in the culture medium. We hypothesize that the size of the aggregates is too large and prevents them from being uptaken by the cells. These results together proved the formation of supramolecular structure in living cells with peptide **2** and underscored the fact that fluorescence method can serve as a valuable tool for imaging SIRT5-mediated self-assembly process of nanofibers. Furthermore, we performed cell imaging experiment of peptide **2** with three different cell lines (HeLa, HepG2 and 3T3). Results indicated that peptide **2** stained HeLa cells and HepG2 cells very well but not 3T3 cells (Figure S12). Two factors could account for this phenomenon. First it could be caused by the different expression level of SIRT5 in different cell lines. Second it could be that the peptide exhibits different cell permeability toward different cell lines.[38,39]

To further confirm that the self-assembly process was selectively triggered by SIRT5, we performed cell inhibition study with suramin. Suramin is an inhibitor of NAD^+-dependent SIRT5.[40] The inhibiting activity of suramin on peptide **2** was first confirmed using HPLC. It was shown that a concentration of 200 μM was sufficient to significantly inhibit the enzymatic activity of SIRT5 (Figure S3d). In addition, cell

https://dx.doi.org/10.1021/jacs.0c08463
J. Am. Chem. Soc. 2020, 142, 18150−18159

viability assay indicated that suramin exhibited low cytotoxicity to HeLa cells (Figure S13). We then performed inhibition studies with live mammalian cells. The cells were preincubated with 300 μM suramin and then incubated with peptide **2**. Significant decrease of intracellular fluorescence was observed (Figure 3c), suggesting that SIRT5 was inhibited and therefore the formation of nanofibers was suppressed. Moreover, siRNA knockdown experiments with HeLa and HepG2 cells showed that fluorescence diminished when SIRT5 was knocked down (Figure S14 and S15). These experiments strongly demonstrate that SIRT5 is the key player for triggering intracellular self-assembly process to form supramolecular nanostructures. In situ self-assembly of fluorescent peptides can be used as a robust chemical tool for imaging SIRT5 activity in living cells. This has not been achieved by small-molecule probe approach.

Self-Assembly Occurred in Mitochondria. To explore whether nanofibers are spatially formed within the mitochondrial region, we conducted colocalization experiments by incubating peptide **2** and MitoTracker Red, a dye used to specifically label mitochondria. As shown in Figures 4a–c and S16, a substantial overlap could be observed between the fluorescence image of NBD-containing nanofibers and that of MitoTracker Red, indicating that the as-formed nanofibers were indeed localized in the mitochondrial region. Moreover, no noticeable NBD fluorescence was observed in the other regions of the cells such as the nucleus. Through further quantitative analysis, the Pearson correlation coefficient was determined to be 0.90 ± 0.006 based on three different cell images.[41,42] The line scan profile (Figure 4d) also proved that the fluorescence from peptide **2** nanofibers overlapped well with that of MitoTracker Red. These data strongly indicate a significant level of colocalization between the two dyes, confirming our hypothesis that peptide **2** is desuccinylated by SIRT5 and primarily self-assemble in the mitochondrial area of cells. Furthermore, we combined cell fractionation and TEM imaging experiment to demonstrate the selective formation of nanofibers in mitochondria. Briefly, we first incubated HeLa cells with peptide **2**, followed by isolating the nucleus, mitochondrial and cytosol fractions via the protocol described in the literature.[30] Further TEM visualization clearly showed that nanofibers were present in the mitochondrial fraction but not in the other fractions such as the nucleus and cytosol (Figures 4e and S17). The size of nanofibers also agreed with that shown in Figure 2c. In addition, control cells incubated without peptide **2** showed only amorphous material (Figure 4f). Combined with both fluorescence and TEM imaging experiments, these data strongly prove that supramolecular nanostructures can be selectively formed in mitochondria with peptide **2**.

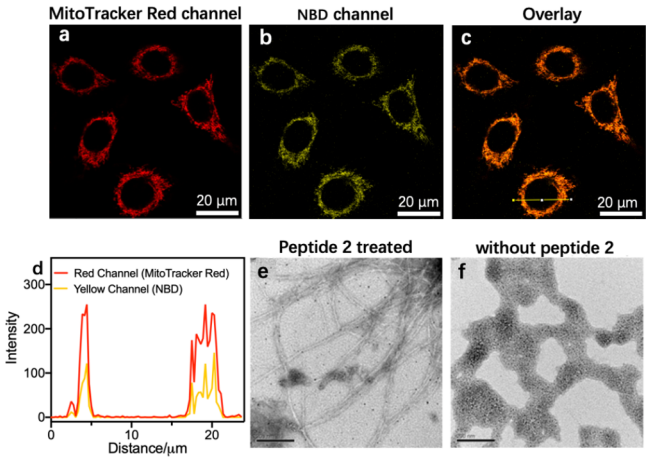

Figure 4. Colocalization and cell fractionation experiments. Fluorescence confocal microscopy images of HeLa cells incubated with 500 μM peptide **2** and 100 nM MitoTracker Red, (a) MitoTracker Red channel; (b) NBD channel; (c) Overlay. Scale bar = 20 μm. (d) Line scan profile of linear region across the HeLa cells in (c). (e) TEM image of mitochondrial fraction following overnight incubation with peptide **2.** (f) TEM image of mitochondrial fraction without overnight incubation of peptide **2.** Scale bar = 200 nm. The images showed very good overlapping between the fluorescence of intracellularly formed nanofibers and that of mitochondria-staining dyes, indicating that the as-formed nanofibers were localized in the mitochondria of cells. TEM images further confirmed the formation of nanofibers in mitochondrial fractions. Moreover, no formation of nanofibers was observed in the control cells.

Self-Assembly Altered Mitochondrial Activity and Induced ROS Formation. To examine whether peptide self-assembly mediated by SIRT5 could modulate mitochondrial activity, we further synthesized an analogue of peptide **2** without a fluorophore, Fmoc-FFFGKsuccG (peptide **5**, Figure 5a). Since this peptide does not contain a fluorophore, it will not interfere with the fluorescence test required in cell imaging experiments.

The desuccinylation activity of peptide **5** by SIRT5 was first examined with HPLC and MS experiments (Figure S18 and S19). Experimental results indicated that more than 85% of peptide **5** could be desuccinylated by SIRT5 efficiently. Next the in vitro self-assembly activity of peptide **5** with SIRT5 was confirmed with hydrogelation and TEM experiments (Figure 5b and S20). Subsequently HeLa cells were incubated with peptide **5** overnight and the mitochondrial fraction was isolated. Indeed, substantial amounts of nanofibers were found in the mitochondrial fractions after treatment of peptide **5** (Figure 5c). On the other hand, no nanofiber was found in control cells without addition of peptide **5** (Figure S21). Moreover, the desuccinylated product of peptide **5** was found in the mitochondrial fractions through ESI-MS analysis, further proving that peptide **5** can be desuccinylated by endogenous SIRT5 in living cells (Figure S22). These results together demonstrate that similar to peptide **2**, peptide **5** can be desuccinylated by endogenous SIRT5 and form nanofiber structures selectively in the mitochondria.

Next we examined whether the mitochondrial activity is affected by in situ nanofiber formation. First we analyzed the membrane potential of the mitochondria through JC-1 staining experiments. JC-1 exists mainly in monomeric form at low concentrations and exhibits green fluorescence. When JC-1 exists at high concentrations, it will form aggregates and give red fluorescence. A fluorescence decrease in aggregated dye channel signifies the depolarization of mitochondria. HeLa cells were incubated with 500 μM peptide **5** for 6 h and then with JC-1 for 20 min before imaging. Subsequently detailed fluorescence imaging study was carried out. As shown in Figure 5d,f, after treating peptide **5** for 6 h, a clear fluorescence decrease in the red channel could be observed with concomitant fluorescence increase in the green channel. These experiments demonstrated that JC-1 existed in increased monomer forms and less aggregation forms, signifying that the mitochondria membrane potential was depolarized due to self-assembly of peptide **5**. Furthermore, cell imaging experiments

https://dx.doi.org/10.1021/jacs.0c08463
J. Am. Chem. Soc. 2020, 142, 18150−18159

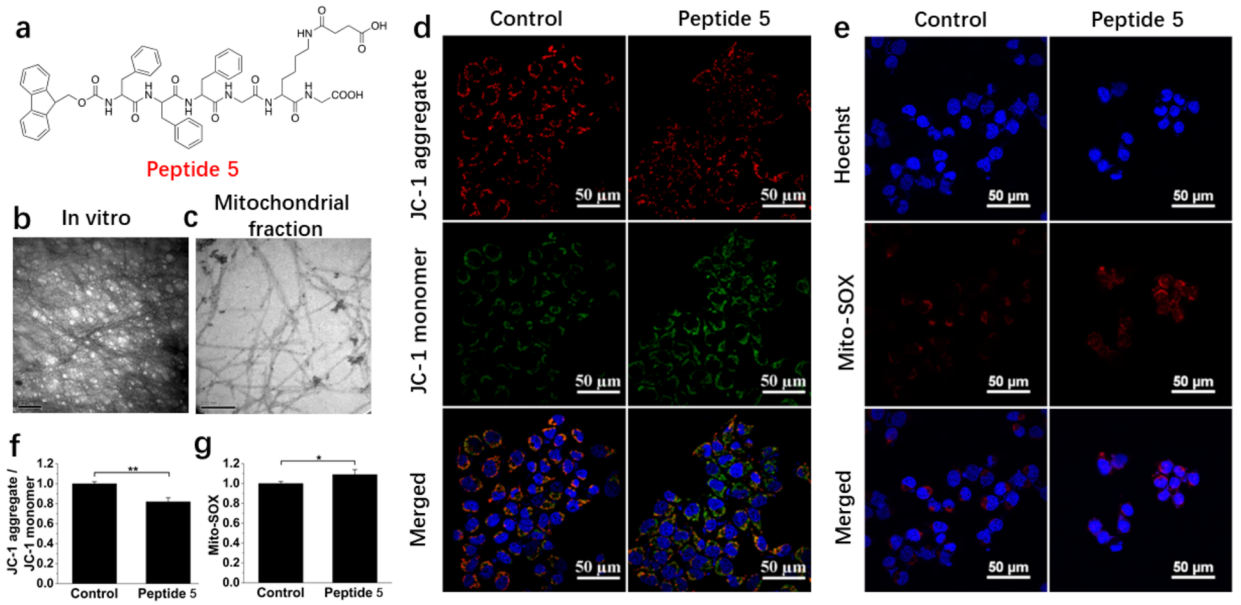

Figure 5. (a) Chemical structure of peptide **5**. (b) TEM image of peptide **5** incubated with SIRT5 and NAD^+ in the buffer. (c) TEM image of mitochondrial fractions after incubation of HeLa cells with peptide **5**. Scale bar = 200 nm. (d) Fluorescence images of JC-1 staining in HeLa cells exposed to 500 μM peptide **5** for 6 h. Scale bar = 50 μm. (e) Fluorescence images of Mito-SOX staining in HeLa cells incubated with 500 μM peptide **5** for 6 h. Control: cells treated with the vehicle without using peptide **5**. Scale bar = 50 μm. (f) Quantitative analysis of the ratios of red fluorescence to green fluorescence in (d), $P = 0.006$. (g) Quantitative analysis of fluorescence intensity in (e), $P = 0.032$. In panels f and g, the fluorescent intensity was quantified by ImageJ software. $^*P < 0.05$ and $^{**}P < 0.01$ between indicated groups (mean ± SD, $n = 3$). $n = 3$ means three different fluorescent images for quantitative analysis.

with Mito-SOX were performed to examine whether mitochondrial ROS was produced with peptide self-assembly. As shown in Figure 5e,g, a clear fluorescence signal increase in Mito-SOX channel was observed in cells treated with peptide **5** compared with that in the control cells, indicating mitochondrial ROS was generated after forming nanofibers in mitochondria. Combined with TEM and cell-based experiments, these results together strongly prove that peptide **5** can form nanofiber structures in mitochondria and attenuate mitochondrial activity accordingly.

Peptide Self-Assembly Enhanced the Anticancer Activities of Different Drugs. After verifying that peptide **5** can self-assemble in mitochondria and alter the mitochondrial activity, we next explored whether SIRT5-mediated self-assembly can be used for combination therapy with anticancer drugs. Literatures have shown that mitochondria play vital roles in apoptosis and can influence the response to chemotherapy drugs.[43−45] In our study, three widely used drugs dichloroacetate (DCA), cisplatin and paclitaxel (Taxol) were selected. The three drugs kill cancer cells with different mechanisms. DCA is a potential anticancer drug that inhibits a key enzyme pyruvate dehydrogenase kinase in mitochondria.[46] Cisplatin is known to interfere with DNA transcription and serves as the first line therapeutic agent for treatment of different cancers.[47] Taxol could bind to tubulin and interfere with cell mitosis, inducing cell apoptosis.[48] In addition, both cisplatin and Taxol have been reported to be associated with mitochondrial activities.[47,48]

We first examined the cytotoxicity of peptide **5** (Figures 6d and S23). The peptide itself at 500 μM concentration showed low cytotoxicity toward HeLa cells after 72 h of incubation, indicating the peptide has good biocompatibility. Gratifyingly, coincubation of peptide **5** and the three drugs significantly boosted their killing ability toward HeLa cells. For instance,

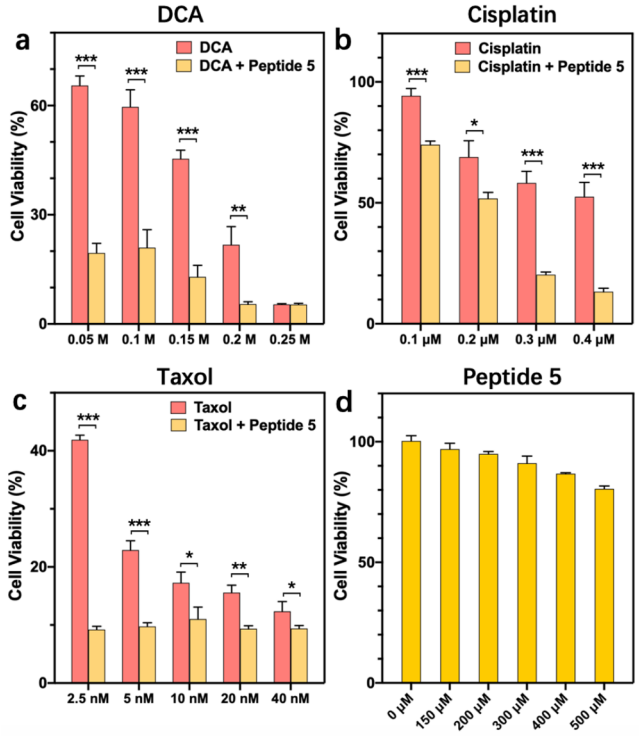

Figure 6. Cell viability assay of HeLa cells incubated with (a) DCA, (b) cisplatin, (c) Taxol with or without 500 μM peptide **5** for 72 h, and (d) peptide **5** (0−500 μM) only. The standard deviation for each data point was averaged over three samples ($n = 3$). $^*P < 0.05$, $^{**}P < 0.01$, and $^{***}P < 0.001$ between indicated groups (mean ± SD, $n = 3$).

https://dx.doi.org/10.1021/jacs.0c08463
J. Am. Chem. Soc. 2020, 142, 18150−18159

coincubation of 0.2 M DCA with peptide **5** led to more than 90% of cell death (Figure 6a). Similarly, using low dosage of cisplatin (0.4 μM) with peptide **5** resulted in more than 80% of cell death (Figure 6b). Coincubation of 2.5 nM Taxol with peptide **5** killed more than 90% cells (Figure 6c). Subsequently, the normalized isobologram and combination index (CI) plot were plotted to analyze the synergistic effects between peptide **5** and different drugs (Figure S24).[49−51] For the combined use of peptide **5** with DCA, all the data points are located on the lower left of the hypotenuse in the isobologram graph(Figure S24a). In addition, the CI values at all concentrations fall into the range of 0.3−0.7, indicating synergistic effect between DCA and peptide **5**. For cisplatin and peptide **5** coincubation, the data points at high concentrations of cisplatin are still located on the lower left of the isobologram graph, showing good synergism (Figure S24b). However, when the concentration of cisplatin decreased to 0.2 μM, the combinations became ineffective. The data points at low concentrations of cisplatin are located on or above the hypotenuse and the CI values are close to or slightly above 1, indicating additive or slight antagonistic effect. For the combinations of Taxol and peptide **5**, all the data points are located on the lower left of the hypotenuse (Figure S24c), and most of the calculated CI values are below 0.5, indicating good synergism between them. Notably, when the concentration of Taxol was less than or equal to 5 nM, it exhibited strong synergism with CI values below 0.2.

The improved killing effects of the drugs might be attributed to the intracellular nanofiber formation and the perturbed mitochondrial activities thereof. The above experiments also demonstrate that SIRT5-mediated self-assembly can serve as a general approach for combination cancer therapy. This method may offer a new strategy for cancer treatment by significantly reducing drug dosage to ameliorate the side effects of drugs during chemotherapy.

CONCLUSION

In summary, we have successfully developed a new approach for guiding supramolecular self-assembly specifically in mitochondria. The supramolecular self-assembly is built on the specific interaction between a new class of succinylated precursors and a mitochondria-localized enzyme. In vitro experiments have demonstrated that SIRT5 can serve as an efficient trigger that selectively catalyzes the transformation of soluble precursors into self-assembling building blocks at physiological pH. The delicate interaction between SIRT5 and the as-designed precursor can be further manifested in mitochondria, as evidenced by the formation of supramolecular nanostructures in a spatially selective manner. Notably, the NBD fluorophore in the formed peptide nanofibers enables activity-based imaging of SIRT5 in living cells for the first time. Furthermore, the formed nanofibers in mitochondria leads to depolarized mitochondrial membranes and increases mitochondria ROS. Subsequent cell viability test proves that the peptide self-assembly can significantly boost the anticancer activities of different drugs. In our study, HeLa cells were used as it is a commonly used cancer cell line. Although SIRT5 level is relatively low in HeLa cells compared with other cancer cell lines, our peptide self-assembly strategy has proved that it can be used to image SIRT5 activity and boost the cell killing activity of drugs in HeLa cells. These applications may be further validated in other cancer cell lines such as SKOV3 cells. On the basis of this study, we envision that our findings can provide new insights for the development of novel supramolecular nanomaterials for mitochondria-targeted cancer therapy.

MATERIAL AND METHODS

Gelation Experiments. Hydrogelation experiments were carried out in glass vials. In a typical experiment, 1 mg of peptide was dissolved in 5 μL of DMSO. SIRT5 (0.005 equiv) and NAD^+ (2 equiv) were then added from stock solutions and the mixture was diluted with Tris buffer or pure water to 100 μL (1 wt %) before the pH was adjusted to 7.4 using concentrated NaOH (typically 1 to 2 μL). After overnight incubation at 37 °C, the samples were allowed to cool to room temperature, and hydrogel was tested by the vial inversion method.

Imaging of Peptide Self-Assembly. Confocal fluorescence images of nanofibers were obtained using peptide solutions at 500 μM in PBS buffer (pH 7.4; 10 mM). Samples were incubated overnight at 37 °C with NAD^+ and SIRT5 (peptide/NAD^+/SIRT5 = 200/400/1) before being thoroughly mixed. A few microliters of solution were deposited between a glass plate and its cover. Fluorescent images were recorded on a Leica TCS SPE Confocal Laser Scanning Microscope using a 100× objective, 458 nm as the excitation wavelength and 495−650 nm as the emission wavelength. TEM samples were prepared by diluting the samples used for confocal imaging by a factor of 10. For each sample, a 10 μL drop was deposited onto a TEM carbon support and allowed to dry overnight. TEM was then conducted on a H7700 transmission electron microscope (Hitachi, Japan).

Live Cell Imaging. The cellular uptake and the intracellular behavior of the studied peptides were characterized using confocal microscopy. Briefly, HeLa cells were seeded in 8-well ibidi culture plates at a density of 15,000 cells/well and allowed to attach to the plate for 12 h in growth medium at 37 °C with 5% CO_2. Subsequently the growth medium was replaced by fresh medium containing appropriate concentrations of peptides and suramin sodium salt. For the time lapse experiment, the cells were imaged immediately and every 3 h afterward. The cells were put back to incubate at 37 °C and 5% CO_2 atmosphere between successive measurements. Fluorescent images were recorded on a Leica TCS SPE Confocal Laser Scanning Microscope using a 40× objective. For NBD dye, 458 nm was used as the excitation wavelength and 495−650 nm as the emission bandwidth. For Hoechst 33342, 405 nm was used as the excitation wavelength and 430−470 nm was used as the emission bandwidth.

For colocalization experiments, HeLa cells were first incubated with peptide **2** (500 μM) overnight before MitoTracker Red (100 nM) was added to the medium from stock solution in DMSO. Following 20 min of incubation, the cells were washed and fresh medium was added for imaging. Fluorescent images were taken using a 100x objective. For the NBD dye, 458 nm was used as the excitation wavelength and 500−600 nm was used as the emission bandwidth. For MitoTracker Red, 543 nm was used as the excitation wavelength and 580−650 nm was used as the emission bandwidth. Colocalization was analyzed using ImageJ software. Colocalization between NBD and the MitoTracker channel were calculated with ImageJ Plugin Coloc 2 on raw data (threshold regression: Costes; PSF: 3.0; Costes randomizations: 10). The averaged Pearson correlation coefficient value was analyzed by selecting three different cell images.

Cell Fractionation Experiments. HeLa cells were incubated with peptide solution (500 μM) overnight. The medium was then removed and the cells were washed with PBS (10 mM, pH 7.4) three times. The cells were then harvested with trypsin, collected, washed with PBS twice and resuspended in PBS containing 0.1% SDS to lyse the cells. Lysis was conducted at room temperature for 30 min. Clumps of unbroken and ruptured cells were removed by centrifugation at 300 g for 5 min, and the supernatant was centrifuged at 600 g for 10 min to obtain nucleus sample. The resultant supernatant was further centrifuged at 15 000*g* for 5 min to obtain the mitochondria sample. HeLa cells treated in the same way but without peptide incubation were used as control.

https://dx.doi.org/10.1021/jacs.0c08463
J. Am. Chem. Soc. 2020, 142, 18150−18159

Mitochondrial Activity Assays. JC-1 kit (Beyotime Biotechnology) was utilized to examine the mitochondrial membrane potential. HeLa cells were incubated with 500 μM peptide **5** for 6 h, followed by staining of JC-1 in the dark for 20 min at 37 °C. The cells were then washed with PBS three times. Next, 5 μg/mL Hoechst 33342 was incubated with HeLa cells at 37 °C for 10 min. After washing with PBS three times, the cells were imaged with a fluorescence microscope. The excitation/emission wavelength for JC-1 monomers is 488/525 nm. The excitation/emission wavelength for JC-1 aggregates is 560/595 nm. In the control group, the cells were treated with the vehicle without using peptide **5**.

Mito-SOX red mitochondrial superoxide indicator (Yeasen Biotech) was used to analyze mitochondrial ROS. HeLa cells were first exposed to 500 μM peptide **5** for 6 h. The cells were then coincubated with Mito-SOX in the dark for 10 min at 37 °C. After staining with 5 μg/mL Hoechst 33342 for 10 min at 37 °C and PBS washing, The HeLa cells were observed with a fluorescence microscope. The excitation/emission wavelength used is 510/580 nm. In the control group, the cells were treated with the vehicle without using peptide **5**.

■ ASSOCIATED CONTENT

Supporting Information

The Supporting Information is available free of charge at https://pubs.acs.org/doi/10.1021/jacs.0c08463.

Additional experimental details, supporting Figures S1−S24, and supplemental references (PDF)

■ AUTHOR INFORMATION

Corresponding Authors

Ming-liang He − *Department of Biomedical Science, City University of Hong Kong, Kowloon, Hong Kong, China*; Email: mlhe7788@gmail.com

Zuankai Wang − *Key Laboratory of Biochip Technology, Biotech and Health Centre, Shenzhen Research Institute of City University of Hong Kong, Shenzhen 518057, China; Department of Mechanical Engineering, City University of Hong Kong, Kowloon, Hong Kong, China*; orcid.org/0000-0002-3510-1122; Email: zuanwang@cityu.edu.hk

Yi Hu − *CAS Key Laboratory for Biomedical Effects of Nanomaterials and Nanosafety, Multidisciplinary Research Division, Institute of High Energy Physics and University of Chinese Academy of Sciences (UCAS), Chinese Academy of Sciences (CAS), Beijing 100049, China*; Email: huyi@ihep.ac.cn

Hongyan Sun − *Department of Chemistry and COSDAF (Centre of Super-Diamond and Advanced Films), City University of Hong Kong, Kowloon, Hong Kong, China; Key Laboratory of Biochip Technology, Biotech and Health Centre, Shenzhen Research Institute of City University of Hong Kong, Shenzhen 518057, China*; orcid.org/0000-0003-0932-6405; Email: hongysun@cityu.edu.hk

Authors

Liu Yang − *Department of Chemistry and COSDAF (Centre of Super-Diamond and Advanced Films), City University of Hong Kong, Kowloon, Hong Kong, China; Key Laboratory of Biochip Technology, Biotech and Health Centre, Shenzhen Research Institute of City University of Hong Kong, Shenzhen 518057, China*

Raoul Peltier − *Department of Chemistry and COSDAF (Centre of Super-Diamond and Advanced Films), City University of Hong Kong, Kowloon, Hong Kong, China; Key Laboratory of Biochip Technology, Biotech and Health Centre, Shenzhen Research Institute of City University of Hong Kong, Shenzhen 518057, China*; orcid.org/0000-0003-0959-8259

Manman Zhang − *Key Laboratory of Biochip Technology, Biotech and Health Centre, Shenzhen Research Institute of City University of Hong Kong, Shenzhen 518057, China; Department of Mechanical Engineering, City University of Hong Kong, Kowloon, Hong Kong, China*

Dan Song − *Department of Biomedical Science, City University of Hong Kong, Kowloon, Hong Kong, China*

Hui Huang − *CAS Key Laboratory for Biomedical Effects of Nanomaterials and Nanosafety, Multidisciplinary Research Division, Institute of High Energy Physics and University of Chinese Academy of Sciences (UCAS), Chinese Academy of Sciences (CAS), Beijing 100049, China*

Ganchao Chen − *Department of Chemistry and COSDAF (Centre of Super-Diamond and Advanced Films), City University of Hong Kong, Kowloon, Hong Kong, China; Key Laboratory of Biochip Technology, Biotech and Health Centre, Shenzhen Research Institute of City University of Hong Kong, Shenzhen 518057, China*

Ying Chen − *Department of Biomedical Science, City University of Hong Kong, Kowloon, Hong Kong, China*

Fanghang Zhou − *Department of Biomedical Science, City University of Hong Kong, Kowloon, Hong Kong, China*

Quan Hao − *School of Biomedical Sciences, University of Hong Kong, Hong Kong, China*

Liming Bian − *Department of Biomedical Engineering, The Chinese University of Hong Kong, Shatin, Hong Kong, China*; orcid.org/0000-0003-4739-0918

Complete contact information is available at: https://pubs.acs.org/10.1021/jacs.0c08463

Author Contributions

◇L.Y., R.P., and M.Z. contributed equally to this work.

Notes

The authors declare no competing financial interest.

■ ACKNOWLEDGMENTS

We are grateful for the financial support from financial support of the Hong Kong Research Grants Council (Nos. 11102719 and 11304118), National Science Foundation of China (Nos. 21778044, 21572190, and 11875269) and the Science Technology and Innovation Committee of Shenzhen Municipality (JCYJ20180507181654823).

■ REFERENCES

(1) Whitesides, G. M.; Mathias, J. P.; Seto, C. T. Molecular self-assembly and nanochemistry: a chemical strategy for the synthesis of nanostructures. *Science* **1991**, *254*, 1312−1319.

(2) Ulijn, R. V. Molecular self-assembly: Best of both worlds. *Nat. Nanotechnol.* **2015**, *10*, 295−296.

(3) Shigemitsu, H.; Hamachi, I. Design strategies of stimuli-responsive supramolecular hydrogels relying on structural analyses and cell-mimicking approaches. *Acc. Chem. Res.* **2017**, *50*, 740−750.

(4) Ikeda, M.; Tanida, T.; Yoshii, T.; Kurotani, K.; Onogi, S.; Urayama, K.; Hamachi, I. Installing logic-gate responses to a variety of biological substances in supramolecular hydrogel-enzyme hybrids. *Nat. Chem.* **2014**, *6*, 511−518.

(5) Zhan, J.; Cai, Y. B.; He, S. S.; Wang, L.; Yang, Z. M. Tandem molecular self-assembly in liver cancer cells. *Angew. Chem., Int. Ed.* **2018**, *57*, 1813−1816.

(6) Hai, Z.; Li, J.; Wu, J.; Xu, J.; Liang, G. Alkaline phosphatase-triggered simultaneous hydrogelation and chemiluminescence. *J. Am. Chem. Soc.* **2017**, *139*, 1041−1044.
(7) Xie, C.; Zhen, X.; Lei, Q.; Ni, R.; Pu, K. Self-assembly of semiconducting polymer amphiphiles for in vivo photoacoustic imaging. *Adv. Funct. Mater.* **2017**, *27*, 1605397.
(8) Wang, H.; Feng, Z.; Xu, B. Bioinspired assembly of small molecules in cell milieu. *Chem. Soc. Rev.* **2017**, *46*, 2421−2436.
(9) Hu, J.; Zhang, G.; Liu, S. Enzyme-responsive polymeric assemblies, nanoparticles and hydrogels. *Chem. Soc. Rev.* **2012**, *41*, 5933−5949.
(10) Wang, H.; Feng, Z.; Xu, B. Assemblies of peptides in a complex environment and their applications. *Angew. Chem., Int. Ed.* **2019**, *58*, 10423−10432.
(11) Ulijn, R. V.; Smith, A. M. Designing peptide based nanomaterials. *Chem. Soc. Rev.* **2008**, *37*, 664−675.
(12) Du, X.; Zhou, J.; Shi, J.; Xu, B. Supramolecular Hydrogelators and Hydrogels: From Soft Matter to Molecular Biomaterials. *Chem. Rev.* **2015**, *115*, 13165−13307.
(13) Zhou, J.; Du, X.; Yamagata, N.; Xu, B. Enzyme-Instructed Self-Assembly of Small D-Peptides as a Multiple-Step Process for Selectively Killing Cancer Cells. *J. Am. Chem. Soc.* **2016**, *138*, 3813−3823.
(14) He, H.; Liu, S.; Wu, D.; Xu, B. Enzymatically-Formed Peptide Assemblies Sequestrate Proteins and Relocate Inhibitors for Selectively Killing Cancer Cells. *Angew. Chem., Int. Ed.* **2020**, *59*, 16445−16450.
(15) Liu, S.; Xu, B. Enzyme-Instructed Self-Assembly for Subcellular Targeting. *ACS Omega* **2020**, *5*, 15771−15776.
(16) Wang, H.; Feng, Z.; Wang, Y.; Zhou, R.; Yang, Z.; Xu, B. Intergrating enzymatic self-assembly and mitochondria targeting for selectively killing cancer cells without acquired drug resistance. *J. Am. Chem. Soc.* **2016**, *138*, 16046−16055.
(17) Jeena, M. T.; Palanikumar, L.; Go, E. M.; Kim, I.; Kang, M. G.; Lee, S.; Park, S.; Choi, H.; Kim, C.; Jin, S. M.; Bae, S. C.; Rhee, H. W.; Lee, E.; Kwak, S. K.; Ryu, J. H. Mitochondria localization induced self-assembly of peptide amphiphiles for cellular dysfunction. *Nat. Commun.* **2017**, *8*, 26.
(18) He, H.; Wang, J.; Wang, H.; Zhou, N.; Yang, D.; Green, D. R.; Xu, B. Enzymatic cleavage of branched peptides for targeting mitochondria. *J. Am. Chem. Soc.* **2018**, *140*, 1215−1218.
(19) He, H.; Guo, J.; Lin, X.; Xu, B. Enzyme-Instructed Assemblies Enable Mitochondria Localization of Histone H2B in Cancer Cells. *Angew. Chem., Int. Ed.* **2020**, *59*, 9330−9334.
(20) Cai, Y.; Shen, H.; Zhan, J.; Lin, M.; Dai, L.; Ren, C.; Shi, Y.; Liu, J.; Gao, J.; Yang, Z. Supramolecular "Trojan Horse" for Nuclear Delivery of Dual Anticancer Drugs. *J. Am. Chem. Soc.* **2017**, *139*, 2876−2879.
(21) Feng, Z.; Wang, H.; Wang, S.; Zhang, Q.; Zhang, X.; Rodal, A. A.; Xu, B. Enzymatic Assemblies Disrupt the Membrane and Target Endoplasmic Reticulum for Selective Cancer Cell Death. *J. Am. Chem. Soc.* **2018**, *140*, 9566−9573.
(22) Wang, H.; Feng, Z.; Del Signore, S. J.; Rodal, A. A.; Xu, B. Active Probes for Imaging Membrane Dynamics of Live Cells with High Spatial and Temporal Resolution over Extended Time Scales and Areas. *J. Am. Chem. Soc.* **2018**, *140*, 3505−3509.
(23) Houtkooper, R. H.; Pirinen, E.; Auwerx, J. Sirtuins as regulators of metabolism and healthspan. *Nat. Rev. Mol. Cell Biol.* **2012**, *13*, 225−238.
(24) Du, J.; Zhou, Y.; Su, X.; Yu, J. J.; Khan, S.; Jiang, H.; Kim, J.; Woo, J.; Kim, J. H.; Choi, B. H.; He, B.; Chen, W.; Zhang, S.; Cerione, R. A.; Auwerx, J.; Hao, Q.; Lin, H. Sirt5 is a NAD-dependent protein lysine demalonylase and desuccinylase. *Science* **2011**, *334*, 806−809.
(25) Hirschey, M. D.; Zhao, Y. Metabolic regulation by lysine malonylation, succinylation, and glutarylation. *Mol. Cell. Proteomics* **2015**, *14*, 2308−2315.
(26) Peng, C.; Lu, Z.; Xie, Z.; Cheng, Z.; Chen, Y.; Tan, M.; Luo, H.; Zhang, Y.; He, W.; Yang, K.; Zwaans, B. M.; Tishkoff, D.; Ho, L.; Lombard, D.; He, T. C.; Dai, J.; Verdin, E.; Ye, Y.; Zhao, Y. The first identification of lysine malonylation substrates and its regulatory enzyme. *Mol. Cell. Proteomics* **2011**, *10*, 012658.
(27) Bringman-Rodenbarger, L. R.; Guo, A. H.; Lyssiotis, C. A.; Lombard, D. B. Emerging roles for SIRT5 in metabolism and cancer. *Antioxid. Redox Signaling* **2018**, *28*, 677−690.
(28) Wang, Y. Q.; Wang, H. L.; Xu, J.; Tan, J.; Fu, L. N.; Wang, J. L.; Zou, T. H.; Sun, D. F.; Gao, Q. Y.; Chen, Y. X.; Fang, J. Y. Sirtuin5 contributes to colorectal carcinogenesis by enhancing glutaminolysis in a deglutarylation-dependent manner. *Nat. Commun.* **2018**, *9*, 545.
(29) Michishita, E.; Park, J. Y.; Burneskis, J. M.; Barrett, J. C.; Horikawa, I. Evolutionarily conserved and nonconserved cellular localizations and functions of human SIRT proteins. *Mol. Biol. Cell* **2005**, *16*, 4623−4635.
(30) Gao, Y.; Shi, J.; Yuan, D.; Xu, B. Imaging enzyme-triggered self-assembly of small molecules inside live cells. *Nat. Commun.* **2012**, *3*, 1033.
(31) Wang, H.; Feng, Z.; Del Signore, S. J.; Rodal, A. A.; Xu, B. Active probes for imaging membrane dynamics of live cells with high spatial and temporal resolution over extended time scales and areas. *J. Am. Chem. Soc.* **2018**, *140*, 3505−3509.
(32) Kauffman, W. B.; Fuselier, T.; He, J.; Wimley, W. C. Mechanism Matters: A Taxonomy of Cell Penetrating Peptides. *Trends Biochem. Sci.* **2015**, *40*, 749−764.
(33) Milletti, F. Cell-Penetrating Peptides: Classes, Origin, and Current Landscape. *Drug Discovery Today* **2012**, *17*, 850−860.
(34) Yang, Z.; Gu, H.; Fu, D.; Gao, P.; Lam, J. K.; Xu, B. Enzymatic formation of supramolecular hydrogels. *Adv. Mater.* **2004**, *16*, 1440−1444.
(35) Peltier, R.; Chen, G.; Lei, H.; Zhang, M.; Gao, L.; Lee, S.; Wang, Z.; Sun, H. The rational design of a peptide-based hydrogel responsive to H_2S. *Chem. Commun.* **2015**, *51*, 17273−17276.
(36) Fleming, S.; Ulijn, R. V. Design of nanostructures based on aromatic peptide amphiphiles. *Chem. Soc. Rev.* **2014**, *43*, 8150−8177.
(37) Yan, X.; Zhu, P.; Li, J. Self-assembly and application of diphenylalanine-based nanostructures. *Chem. Soc. Rev.* **2010**, *39*, 1877−1890.
(38) Mueller, J.; Kretzschmar, I.; Volkmer, R.; Boisguerin, P. Comparison of Cellular Uptake Using 22 CPPs in 4 Different Cell Lines. *Bioconjugate Chem.* **2008**, *19*, 2363−2374.
(39) Gronewold, A.; Horn, M.; Ranđelović, I.; Tóvári, J.; Muñoz Vázquez, S.; Schomäcker, K.; Neundorf, I. Characterization of a Cell-Penetrating Peptide with Potential Anticancer Activity. *ChemMedChem* **2017**, *12*, 42−49.
(40) Schuetz, A.; Min, J.; Antoshenko, T.; Wang, C. L.; Allali-Hassani, A.; Dong, A.; Loppnau, P.; Vedadi, M.; Bochkarev, A.; Sternglanz, R.; Plotnikov, A. N. Structural basis of inhibition of the human NAD^+-dependent deacetylase SIRT5 by suramin. *Structure* **2007**, *15*, 377−389.
(41) Dunn, K. W.; Kamocka, M. M.; McDonald, J. H. A practical guide to evaluating colocalization in biological microscopy. *Am. J. Physiol. Cell Physiol.* **2011**, *300*, C723−C742.
(42) Bolte, S.; Cordelieres, F. P. A guided tour into subcellular colocalization analysis in light microscopy. *J. Microsc.* **2006**, *224*, 213−232.
(43) Vyas, S.; Zaganjor, E.; Haigis, M. C. Mitochondria and cancer. *Cell* **2016**, *166*, 555−566.
(44) Zielonka, J.; Joseph, J.; Sikora, A.; Hardy, M.; Ouari, O.; Vasquez-Vivar, J.; Cheng, G.; Lopez, M.; Kalyanaraman, B. Mitochondria-Targeted Triphenylphosphonium-Based Compounds: Syntheses, Mechanisms of Action, and Therapeutic and Diagnostic Applications. *Chem. Rev.* **2017**, *117*, 10043−10120.
(45) Wang, D. Q.; Huang, H.; Zhou, M. X.; Lu, H. R.; Chen, J.; Chang, Y. T.; Gao, J. M.; Chai, Z. F.; Hu, Y. A thermoresponsive nanocarrier for mitochondria-targeted drug delivery. *Chem. Commun.* **2019**, *55*, 4051−4054.
(46) Tataranni, T.; Piccoli, C. Dichloroacetate (DCA) and Cancer: An Overview towards Clinical Applications. *Oxid. Med. Cell. Longevity* **2019**, *2019*, 1.

https://dx.doi.org/10.1021/jacs.0c08463
J. Am. Chem. Soc. 2020, 142, 18150−18159

(47) Kleih, M.; Bopple, K.; Dong, M.; Gaissler, A.; Heine, S.; Olayioye, M. A.; Aulitzky, W. E.; Essmann, F. Direct impact of cisplatin on mitochondria induces ROS production that dictates cell fate of ovarian cancer cells. *Cell Death Dis.* **2019**, *10*, 851.
(48) Chavez, J. D.; Keller, A.; Zhou, B.; Tian, R.; Bruce, J. E. Cellular Interactome Dynamics during Paclitaxel Treatment. *Cell Rep.* **2019**, *29*, 2371−2383.
(49) Chou, T. C. Preclinical versus clinical drug combination studies. *Leuk. Lymphoma* **2008**, *49*, 2059−2080.
(50) Chou, T. C. Drug combination studies and their synergy quantification using the Chou-Talalay method. *Cancer Res.* **2010**, *70*, 440−446.
(51) Zhou, J.; Du, X. W.; Chen, X. Y.; Wang, J. Q.; Zhou, N.; Wu, D. F.; Xu, B. Enzymatic self-assembly confers exceptionally strong synergism with NF-κB targeting for selective necroptosis of cancer cells. *J. Am. Chem. Soc.* **2018**, *140*, 2301−2308.

https://dx.doi.org/10.1021/jacs.0c08463
J. Am. Chem. Soc. 2020, 142, 18150−18159